



Strong methane point sources contribute a disproportionate fraction of total emissions across multiple basins in the United States

Daniel H. Cusworth^{a,b,1} , Andrew K. Thorpe^c, Alana K. Ayasse^{a,b} , David Stepp^b, Joseph Heckler^d, Gregory P. Asner^{d,b} , Charles E. Miller^c , Vineet Yadav^c , John W. Chapman^c, Michael L. Eastwood^c, Robert O. Green^c, Benjamin Hmiel^e , David R. Lyon^e , and Riley M. Duren^{a,b,c} 

Edited by Venkatachalam Ramaswamy, NOAA/ GFDL, Princeton, NJ; received February 9, 2022; accepted July 20, 2022 by Editorial Board Member Robert E. Dickinson

Understanding, prioritizing, and mitigating methane (CH₄) emissions requires quantifying CH₄ budgets from facility scales to regional scales with the ability to differentiate between source sectors. We deployed a tiered observing system for multiple basins in the United States (San Joaquin Valley, Uinta, Denver-Julesburg, Permian, Marcellus). We quantify strong point source emissions (>10 kg CH₄ h⁻¹) using airborne imaging spectrometers, attribute them to sectors, and assess their intermittency with multiple revisits. We compare these point source emissions to total basin CH₄ fluxes derived from inversion of Sentinel-5p satellite CH₄ observations. Across basins, point sources make up on average 40% of the regional flux. We sampled some basins several times across multiple months and years and find a distinct bimodal structure to emission timescales: the total point source budget is split nearly in half by short-lasting and long-lasting emission events. With the increasing airborne and satellite observing capabilities planned for the near future, tiered observing systems will more fully quantify and attribute CH₄ emissions from facility to regional scales, which is needed to effectively and efficiently reduce methane emissions.

methane | fossil fuel | imaging spectroscopy | inversion | livestock

Due to its short atmospheric lifetime and strong contribution to global radiative forcing, methane (CH₄) has been a focus for near-term climate mitigation efforts (1). Robust, unbiased accounting systems are requisite to prioritizing and validating CH₄ mitigation, ideally from multiple independent data streams. Atmospheric observations of CH₄ can be key for mitigation, as observed CH₄ concentrations are used to quantify emission rates and attribute emissions to sources. Findings from many independent research efforts have shown that CH₄ emissions across multiple sectors follow heavy-tailed distributions (2–5), meaning that a small fraction of emission sources emits at disproportionately higher rates than the full population of emitters. CH₄ sources can be intermittent or persistent in duration, which may be associated with short-lasting process-driven releases or long-lasting emissions due to abnormal or otherwise avoidable operating conditions such as malfunctions or leaks (5). Isolating populations of large emitters at varying levels of intermittency while quantifying their contribution to regional budgets creates a clear direction for mitigation focus. This tiered observing system strategy can be deployed in data-rich regions where multiple independent layers of observations are jointly leveraged to quantify and isolate emissions, and then drive action.

Advances in CH₄ remote sensing have enabled quantification of emissions from global to facility scales. Generally, these observing systems operate by measuring solar backscattered radiance in shortwave infrared regions where CH₄ is a known absorber. Global mapping satellite missions have been used to identify CH₄ hotspots and infer global- to regional-scale CH₄ emission fluxes (6–8). In particular, the Tropospheric Monitoring Instrument [TROPOMI (9)] onboard the Sentinel-5p satellite has proven capable of quantifying fluxes at basin scales (10, 11). Due to the kilometer-scale resolution of measurements from these global mapping missions, further attribution to particular facilities or even emission sectors is often not feasible. Less precise, target-mode satellites [e.g., PRISMA (12), GHGSat (13)] have proven capable of quantifying very large emissions at an ~30-m scale, allowing for direct emission attribution to facilities or even subfacility-level infrastructure. However, the current generation of CH₄ plume imaging satellites lack the spatial and temporal coverage to provide quantification completeness across multiple basins. For global mapping, high-spatial resolution multispectral satellites such as Sentinel-2 and Landsat are capable of CH₄ detection (14, 15), but only for large emission sources (e.g., 2+ t h⁻¹) over very bright surfaces.

Significance

Large methane point sources exist across multiple source sectors (e.g., oil, gas, coal, livestock, waste). Lacking is a robust assessment of the relative contribution of strong methane point sources against total or regional budgets, which is needed for prioritizing mitigation. In this study, we flew airborne imaging spectrometers repeatedly over multiple basins in the United States to quantify large methane point sources across multiple sectors. We compared these point sources to satellite-based regional flux inversions and found that methane super-emitters consistently make up a sizable contribution to total the total flux in a basin. These results show that a significant climate benefit can be realized by specific isolation and remediation of relatively few sources.

Author contributions: D.H.C., A.K.T., and R.M.D. designed the study and airborne surveys; A.K.A., D.S., V.Y., B.H., and D.R.L. performed analyses and quality control of airborne or inversion results; J.H., G.P.A., J.W.C., M.L.E., and R.O.G. provided airborne and in-field support for airborne campaigns; V.Y. helped set up the CH₄ flux inversion framework on high-performance computers; D.H.C. wrote the manuscript. All authors provided feedback and comments on the manuscript.

The authors declare no competing interest.

This article is a PNAS Direct Submission. V.R. is a Guest Editor invited by the Editorial Board.

Copyright © 2022 the Author(s). Published by PNAS. This open access article is distributed under Creative Commons Attribution-NonCommercial-NoDerivatives License 4.0 (CC BY-NC-ND).

¹To whom correspondence may be addressed. Email: dcusworth@arizona.edu.

This article contains supporting information online at <http://www.pnas.org/lookup/suppl/doi:10.1073/pnas.2202338119/-DCSupplemental>.

Published September 13, 2022.

Airborne imaging spectrometers with shortwave infrared sensitivities and sufficient instrument signal-to-noise ratios can also quantify column CH_4 concentrations. These remote sensing platforms are capable of resolving CH_4 concentrations at high spatial resolution (~ 3 to 5 m) depending on flight altitude, and can quantify point source emissions as low as 5 to 10 kg h^{-1} (16, 17). These instruments are sensitive to concentrated point-source emissions, and less sensitive to diffuse emissions spread over large areas (e.g., wetlands). Given the heavy-tailed nature of anthropogenic emissions, point-source detections above an imaging spectrometer's detection limit may constitute a sizable fraction of the total regional CH_4 flux, but independent measurements are needed to provide that context. Therefore, in this study, we flew a combination of the Global Airborne Observatory (GAO) and next-generation Airborne Visible/Infrared Imaging Spectrometer (AVIRIS-NG) over multiple CH_4 emitting regions between 2019 and 2021, including the southern San Joaquin Valley (SJV), the Permian, the Denver-Julesburg (DJ), the Uinta, and the southwestern Pennsylvania portion of the Marcellus. We generally mapped each basin at least three times during each campaign to quantify persistence of emission sources. For the Permian, DJ, and SJV, we surveyed each region again after several months to assess trends and identify long-lasting emission sources. We also performed simultaneous regional CH_4 flux inversions based on TROPOMI CH_4 retrievals to quantify the total CH_4 flux for each survey and

compared against the quantified airborne point source budgets. With this tiered approach, we are able to quantify the contribution of unique point sources by sector on the regional budget, therefore highlighting specific points of action for mitigation.

Results and Discussion

Point and Regional CH_4 Budgets across Multiple Basins. Fig. 1A shows the results from the multibasin surveys, including persistence-adjusted point source emissions (see *Materials and Methods*) compared against 1) total CH_4 fluxes we derived simultaneously from a regularized inversion of TROPOMI XCH_4 column concentrations (methods described in *SI Appendix, Section S2.1*) (18), and 2) bottom-up gridded emission inventories for oil and gas (O&G), other anthropogenic, and natural sources (19–21). Our CH_4 flux inversion approach has been validated using independent flux estimates from multiple basins (*SI Appendix, Section S2.2*), and the gridded results for each inversion are shown in *SI Appendix, Figs. S2–S4*. All emission estimates are normalized to the area covered by each survey (Table 1). We find that across all basin and time periods, point sources make up on average 40% of each basin's total flux. This occurs both in O&G-dominant basins (Permian, Uinta), but also in basins with more differentiated sources (Marcellus, DJ, SJV). In particular, in the surveyed area of the Marcellus basin, we ascribe 58% of the regional flux to point sources, which is driven primarily by

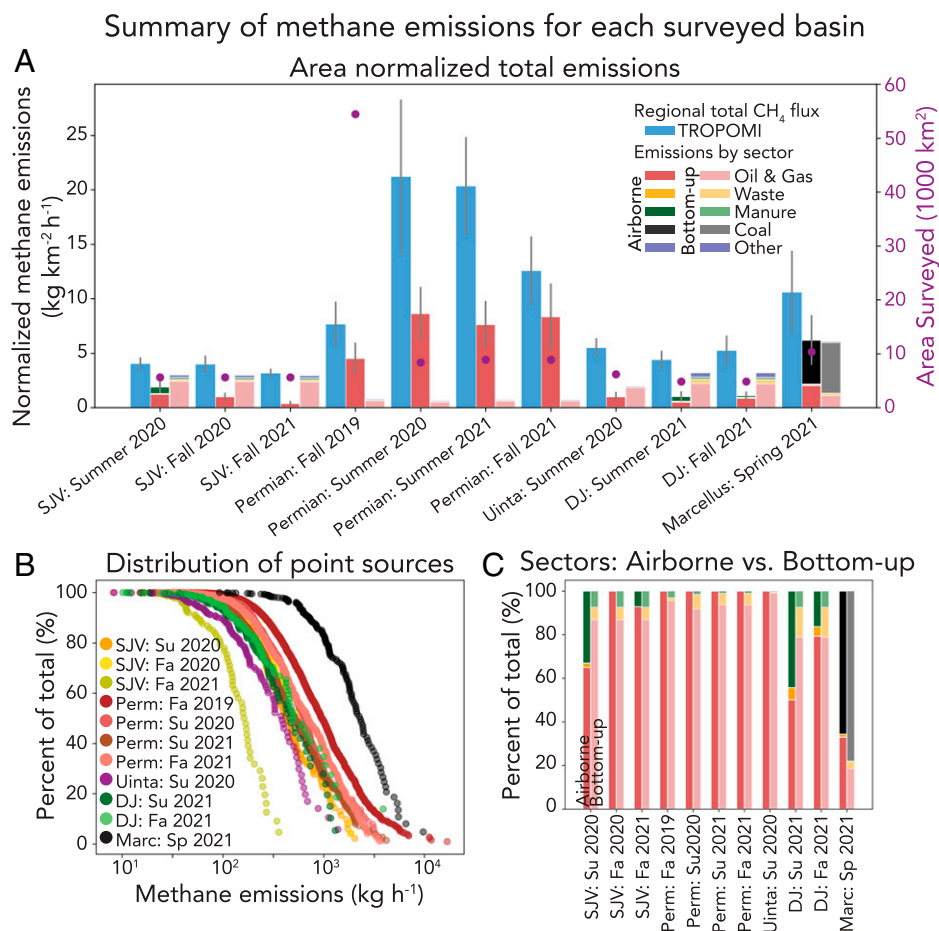


Fig. 1. Summary statistics for each basin surveyed between 2019 and 2021. (See Fig. 3.) (A) Comparison between aggregated point source emissions for each campaign with a top-down spatially/temporally synchronous TROPOMI flux inversion and bottom-up emission from the 2012 EPA gridded inventory. (B) Cumulative distribution of airborne plume emissions quantified for each campaign. (C) Relative sector breakdown between airborne plume emissions and the bottom-up inventory for the following emission sectors: oil and gas (dark/light red), waste management (dark/light yellow), manure management (dark/light green), and coal (dark/light black).

Table 1. Summary of basins surveyed and CH₄ results

Basin	Dates surveyed	Area surveyed (km ²)	No. of detected plumes	Total airborne CH ₄ emissions (t h ⁻¹)*	Sector contribution to point source total (%) [†]	Average no. of overpasses per source	Average source persistence (unitless)	Total area CH ₄ flux (t h ⁻¹) [‡]	Contribution of point sources to area flux (%)
San Joaquin Valley	July 8 to September 24, 2020	5,600	284	10.6 ± 3.3	O: 65 W: 2 M: 33 C: 0	8.2	0.29	22.5 ± 3.3	47
San Joaquin Valley	November 9–23, 2020	5,600	111	5.56 ± 2.0	O: 100 W: 0 M: 0 C: 0	6.2	0.28	22.2 ± 4.5	25
San Joaquin Valley	November 5–13, 2021	5,600	68	2.34 ± 3.3	O: 93 W: 0 M: 7 C: 0	3.1	0.41	17.6 ± 2.4	13
Permian	September 22 to November 4, 2019	54,000	3025	246 ± 79	O: 100 W: 0 M: 0 C: 0	7.7	0.26	415 ± 110	59
Permian	July 13–24, 2020	8,400	595	72.3 ± 20	O: 100 W: 0 M: 0 C: 0%	3.2	0.45	177 ± 59	41
Permian	July 26 to August 10, 2021	8,900	901	67.7 ± 19	O: 100 W: 0 M: 0 C: 0	3.9	0.39	181 ± 40	38
Permian	October 3–17, 2021	8,900	765	74.1 ± 27	O: 100 W: 0 M: 0 C: 0	4.0	0.38	111 ± 28	67
Uinta	July 26 to August 7, 2020	6,200	123	6.13 ± 2.8	O: 100 W: 0 M: 0 C: 0	3.6	0.44	33.9 ± 5.5	18
Denver-Julesburg	July 12–22, 2021	4,800	92	4.98 ± 2.1	O: 50 W: 6 M: 44 C: 0	4.5	0.34	21.1 ± 4.1	24
Denver-Julesburg	September 19–29, 2021	4,800	94	5.37 ± 1.7	O: 79 W: 5 M: 16 C: 0	4.8	0.28	25.2 ± 6.8	21
Southwest Pennsylvania	May 13–21, 2021	10,300	136	63.8 ± 24	O: 33 W: 1 M: 0 C: 66	3.1	0.60	109 ± 39	59

*Total airborne emissions calculated by aggregated persistence-averaged source emissions within each observing domain.

[†]O, O&G; W, waste management; M, wet manure management; C, coal.

[‡]Total area flux estimated through inversion of TROPOMI XCH₄ (methods described in *SI Appendix, Section S2*).

persistent coal mine venting that makes up 65% of the point source budget. Venting is an expected and permitted operation, but is a major contributor to regional and national greenhouse gas emissions. The coal venting operations we quantified just in the southwestern portion of Pennsylvania together represent $0.36 \pm 0.13 \text{ Tg a}^{-1}$. This constitutes 1.3% of the US Environmental Protection Agency (EPA)'s national CH₄ bottom-up inventory for 2019 (26.9 Tg) and 3.4% of the national energy sector emission estimates (10.7 Tg), which includes all fossil-fuel CH₄ sources (22).

Fig. 1A shows that the bottom-up inventory generally underestimates the total CH₄ flux derived from TROPOMI, a result consistent with previous top-down analyses (23). This discrepancy is due to several factors, including the age of the inventory (2012 to 2016) which may underestimate current activity information and emission factors, especially for O&G basins with increasing production (e.g., the Permian). Geospatial information included in the inventory may also be inaccurate or outdated, which biases comparisons to surveys that only look at subregions of full basins. However, Fig. 1C shows the relative contribution

of O&G, waste, manure management, and coal emissions in each region, as quantified by our airborne surveys and the bottom-up inventory. Here, relative contributions are more consistent with the bottom-up inventory across campaigns. A few caveats apply, especially in regard to manure management. For example, during the July 2021 DJ survey, the contributions from point source manure emissions (44% ; $2,200 \pm 970 \text{ kg h}^{-1}$) were nearly equal to O&G emissions (50% ; $2,490 \pm 1,100 \text{ kg h}^{-1}$). When the basin was resurveyed in September to October 2021, the contribution from manure was only $875 \pm 280 \text{ kg h}^{-1}$ or 16% of the total ($5,370 \pm 1,700 \text{ kg h}^{-1}$), due to both a reduction in manure emissions and an increase in O&G emissions (79% ; $4,250 \pm 1,400 \text{ kg h}^{-1}$). The bottom-up inventory estimates only 6.5% of emissions from manure in this same region, an underestimate compared to either airborne DJ survey. According to measurements from the Greely Airport (24), the average local noontime temperature dropped 5°C between summer and fall campaigns. More study is needed to verify if seasonal variability can explain the apparent discrepancy with the bottom-up inventory or if manure management is a much larger relative emitter than expected.

Table 2 lists observed O&G point sources by upstream and midstream supply-chain segments, including production site (well site or tank battery at well site), pipeline (mostly gathering with some transmission), compression (gathering and transmission), processing plants, and other or unidentifiable O&G infrastructure. For every survey, production makes up the majority of the O&G emission budget, although its contribution is highly variable, ranging from 39 to 82% . Compression and processing make up a smaller percentage of the budget (7.1 to 35% and

0 to 11% , respectively), which is consistent with top-down studies (23). One discrepancy is in the Permian Basin, where compression and processing represent 19 to 35% and 6 to 11% of the O&G budget, respectively. The higher concentration of emissions in the midstream sector in the Permian is a result observed previously and is likely the result of insufficient haul-away capacity to match the fast increase in production in the basin (5, 25).

Timescales of Short- and Long-Lasting Emission Sources. In Fig. 1, we use frequency of plume detections (i.e., persistence) to calculate time-averaged emission rates at each source location. A related metric is the timescale of each emission source for sources where multiple plumes were detected across independent flight days. We define source timescale as the length of time between the first and the last plume detection for a given source. In order to compare across multiple campaigns, we normalize timescales by the length of their respective campaign or campaigns. For example, if the timescale of a source is 6 d for a 10-d campaign, then the normalized timescale is 0.6 . Due to revisit feasibility during field campaigns, not every source can be flown on the first and last days of each campaign, so this normalization may artificially shorten timescales. However, this potential source of bias becomes negligible when looking at field campaigns across multiple months and years.

Fig. 2 shows the distribution of emission source timescales for individual campaigns. The distribution of timescales for individual campaigns (Fig. 2A) is nearly flat, but shows a slight decrease as timescales get longer, except for a small jump around 0.8 , due to persistent coal venting emissions in the Marcellus (Table 1).

Table 2. Oil and gas emission contributions from various supply chain components

Basin	Dates surveyed	O&G point source total (t h^{-1})	Production (%)	Compression (%)	Gathering pipelines (%)	Processing (%)	Other (%)
San Joaquin Valley	July 8 to September 24, 2020	6.92 ± 2.1	43	7	45	0	5
San Joaquin Valley	November 9–23, 2020	5.56 ± 2.0	39	16	41	2	2
San Joaquin Valley	November 5–13, 2021	2.17 ± 1.0	66	11	23	0	0
Permian	September 22 to November 4, 2019	246 ± 79	50	19	23	9	0
Permian	July 13–24, 2020	72.3 ± 20	39	35	20	6	0
Permian	July 26 to August 10, 2021	67.7 ± 19	43	31	19	7	0
Permian	October 3–17, 2021	74.1 ± 27	47	33	9	11	1
Uinta	July 26 to August 7, 2020	6.13 ± 2.8	59	2	34	5	0
Denver-Julesburg	July 12–22, 2021	2.54 ± 1.1	71	12	7	9	0
Denver-Julesburg	September 19–29, 2021	4.25 ± 1.4	51	13	28	9	0
Southwest Pennsylvania	May 13–21, 2021	20.9 ± 7.8	82	15	3	0	0
Average across campaigns			53	18	23	5	1

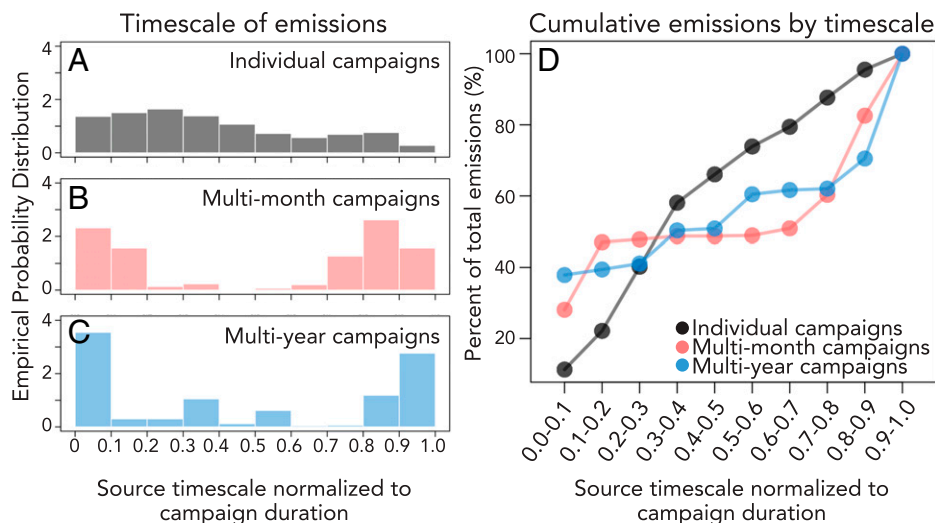


Fig. 2. Timescale or duration of emission sources. (A) Normalized source timescale (quantified duration of an emission event divided by length of campaign) of emissions across all campaigns. (B) Normalized source timescale for multimonth campaigns (i.e., 2020 summer/fall San Joaquin Valley; 2021 summer/fall Permian Basin; 2021 summer/fall Denver-Julesburg Basin). (C) Normalized source timescale for multiyear campaigns (i.e., 2020 to 2021 San Joaquin Valley; 2019 to 2021 Permian Basin). (D) Cumulative emissions binned by normalized source timescales for A–C.

This overall flat structure is likely due to sampling conditions during individual campaigns; uniform revisit frequency for sources within campaigns is often technically infeasible given weather and other logistical considerations. Therefore, we also calculate source timescales for multimonth (DJ summer/fall 2021; Permian summer/fall 2021; SJV summer/fall 2020) and multiyear campaigns (Permian 2019 to 2021; SJV 2020 to 2021) by reclustering plumes to emission sources across the longer multimonth or year temporal domain (Fig. 2 B and C). For multimonth campaigns, a clear bimodal structure appears centered around short timescales (0 to 0.2) and long timescales (0.7 to 1.0). The bimodal structure persists for multiyear campaigns (Permian 2019 to 2021; SJV 2020 to 2021), showing that some sources show sustained emission activity over long timescales.

Sources with both short and long timescales contribute significant fractions to total emissions. Fig. 2D shows the cumulative contribution of emissions from each normalized timescale bin to the total. For multimonth and year campaigns, sources with normalized timescales greater than 0.7 contribute 38 to 39% to the total. Short-lasting sources (0 to 0.3 normalized timescale) contribute 41 to 48% to the total. For effective mitigation, this means that within the point source population of emissions, top-down monitoring solutions need temporal sampling capability to capture both source timescales. Long-lasting sources may be indicative of leaks, malfunctions, or some known releases (e.g., permitted coal venting). Short-lasting sources may be indicative of expected releases (e.g., temporary maintenance) or malfunctions triggered by variable process conditions (e.g., pressure buildup). A revisit strategy with long revisit intervals (e.g., months) would not be able to easily distinguish between these timescale categories and could potentially miss a sizable contribution from short-lasting emission sources.

Emission Trends. The multiyear campaigns in the Permian and SJV allow us to look at basin-scale trends. In the Permian, the spatial overflight domains across campaigns are not consistent. The fall 2019 campaign mapped a much wider area of the Permian, and subsequent campaigns in 2020 to 2021 focused on areas of large activity that were originally identified in 2019. We therefore look at just the overlapping regions flown among all campaigns. Within the region of overlap (SI Appendix, Fig. S5),

the point-source aggregated emissions from 2019 are much higher ($0.84 \pm 0.27 \text{ Tg a}^{-1}$) than in subsequent revisits in summer 2020, summer 2021, and fall 2021 ($0.52 \pm 0.15 \text{ Tg a}^{-1}$, $0.41 \pm 0.12 \text{ Tg a}^{-1}$, and $0.48 \pm 0.19 \text{ Tg a}^{-1}$, respectively). Reduction from high fall 2019 CH₄ emissions, quantified by both airborne and satellite data, may be due to multiple causes. COVID-19 and oil market impacts were previously observed to correlate with reduced flaring activity and fewer well completions, which can impact CH₄ emissions (25). In addition, since 2019, aerial and ground-based data generated from this and other studies have been shared with operators on an ongoing basis (e.g., via [PermianMap.org](https://permianmap.org)). Other operators have funded independent aerial measurements and have claimed emission reductions based on those results [e.g., ExxonMobil (26)]. Another cause could be the heterogeneity of operators, leases, and supply chain activity in the Permian contributing to general high variability in emissions. For example, fall 2019 aggregated Permian airborne point-source emissions were as much as a factor of 2 variable on daily to weekly timescales (5). More long-term trend and attribution analysis is needed to disentangle trends from general variability for the Permian.

A strong relative reduction (69 to 76%) in point-source emissions occurred in SJV between summer 2020 and fall 2021, along with a 20% reduction in the total flux (Table 1). This also corresponds to an 81% emission reduction for point sources in SJV observed with AVIRIS-NG during the California Methane Survey ($12,600 \pm 3,700 \text{ kg h}^{-1}$) (4). The decrease in emissions is driven by reductions in both the O&G and livestock sectors. Since 2016, many digesters (impermeable liners) were placed over manure lagoons across multiple dairies in southern Kern County (27). This appears to have had a sizable impact, as emissions from this sector reduced in summer 2021 from $3,500 \pm 1,100 \text{ kg h}^{-1}$ to $166 \pm 77 \text{ kg h}^{-1}$ in 2021. There was not complete overlap in these regions across campaigns, and dairies were not sampled during the fall 2020 campaign. However, almost all manure CH₄ sources detected in summer 2020 were reflowed in fall 2021. This indicates that the trend is not biased from sampling, although there could be a contribution from seasonality of emissions, which may also be driving manure emission variability in the DJ basin. O&G emissions dropped from 6,920 to 5,560 kg h⁻¹ between summer and fall 2020 campaigns

to $2,170 \pm 1,000 \text{ kg h}^{-1}$ in 2021. During the fall 2020 campaign, researchers from the California Air Resources Board, Carbon Mapper, and NASA JPL shared CH_4 plume detections with individual operators and solicited feedback regarding causes of emissions and any mitigation efforts. Reductions in emissions between 2020 and 2021 could be driven by this outreach effort, although sustained monitoring is needed to confirm that sources remain low or nonemitting into the future.

Conclusions

No single instrument, measurement platform, or network is capable of full characterization of CH_4 emissions within a basin or region. Therefore, tiered observing systems are needed to adequately constrain emission budgets and prioritize areas and infrastructure for mitigation. We demonstrated an application of this system using remote sensing platforms across multiple basins in the United States during 2019 to 2021. The results from this multibasin tiered analysis show that point sources make up around 40% of the total CH_4 flux (13 to 67% range) and highlight the heavy-tailed nature of point sources across many regions and sectors. It is likely that if a basin is known to be made of up of any combination of emission sectors that are characteristically heavy tailed (e.g., O&G, coal, manure management, waste), there is a strong likelihood that point sources will make up a significant fraction of the entire region's emissions.

We show that sources that emit over short and long time-scales equally contribute to point source budgets, which has implications for designing monitoring strategies. Therefore, the global scalability of tiered observing systems depends on the completeness of atmospheric observations, which entails sensitivity to emissions, temporal revisit, and spatial completeness (28). In addition to aircraft campaigns, point-source quantification will rapidly expand with emerging satellite missions (e.g., Carbon

Mapper; 2023 launch). Total basin flux estimation will also improve with wide-swath mapping missions (e.g., MethaneSat; 2023 launch). Where available, ground-based networks are also critical for quantifying regional emissions (29) and for validation of remote-sensing platforms. As these data products are refined and made freely available to the public in easily interpretable formats, there exists great potential in handing off atmospherically informed datasets to appropriate operators and agencies to ultimately reduce CH_4 emissions.

Materials and Methods

Detailed descriptions of plume-level quality control protocols and TROPOMI flux algorithms and validation are described in the *SI Appendix*. Survey design and plume aggregation methods are described below.

Survey Design. We mapped five distinct basins using GAO and/or AVIRIS-NG from 2019 to 2021 (Fig. 3). AVIRIS-NG and GAO are similarly built instruments that measure solar backscatter between 380 and 2,500 nm at 5-nm spectral resolution. CH_4 concentrations were retrieved in the 2,200 to 2,400 nm CH_4 -absorbing region using a column-wise matched filter algorithm (5). Plumes were identified by visual inspection, whose protocols are described in the *SI Appendix, Section S1*. Emission rates and uncertainties were quantified using an integrated methane enhancement (IME) algorithm that has been validated against multiple controlled release experiments and independent in situ measurement (4, 16, 17). Fig. 3 shows example plumes that were detected across multiple basins and across unique sectors. Emission sectors with point source plume characteristics detectable by AVIRIS-NG/GAO include O&G, wet manure management from animal feedlots, waste management from high-capacity landfills, and coal mine seepage/venting. Other diffuse emissions, including enteric fermentation, dry manure management, and wetlands, are not easily detectable with this type of imaging spectrometer. Table 1 provides summary information for each basin, including dates and area flown, number of detected plumes, and estimated emissions. *SI Appendix, Fig. S1* shows each domain and the specific flight line outlines for each survey.

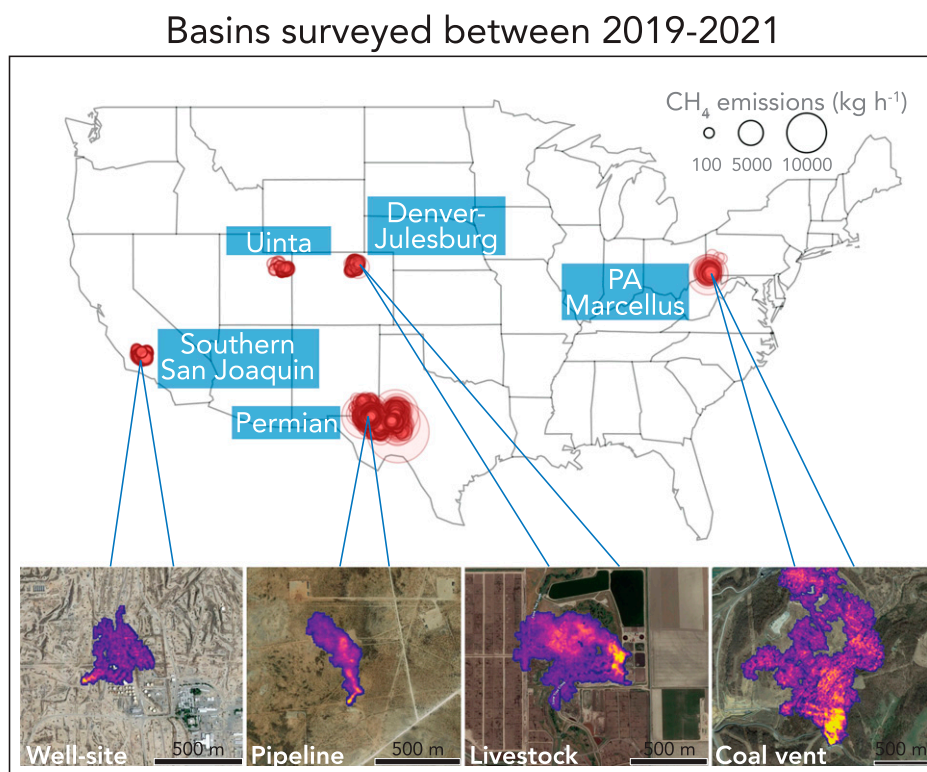


Fig. 3. Major basins surveyed between 2019 and 2021 with either the GAO or AVIRIS-NG airborne imaging spectrometers. *Bottom panels* show representative CH_4 point source plumes from various emission sources, including a well site, pipeline, manure management/livestock, and a coal vent.

Source Aggregation and Persistence Calculations. To generate aggregate statistics for plumes that originate from the same facilities, each quantified plume is clustered in space and time with any other detection within 150 m, a typical lateral distance of a well site that is also within the geolocation uncertainty of the instrument (6 to 10 m). This process clusters plumes into sources, which can be attributed to facilities or infrastructure. GAO has a boresighted high-resolution (~0.6 m) digital airborne camera that we use to attribute sources to specific sectors. For AVIRIS-NG, we use a combination of 3- to 5-m RGB (red, green, blue) channels from the imaging spectrometer and Google Earth base imagery for source attribution. For sources with at least three overflights, we apply persistence weighting to estimate average emissions. This weighting scales the average emission rate by persistence (f), or by the number of detections (M) divided by N , the number of overflights ($f = M/N$). We consider three overflights to be the minimum needed to detect a characteristically intermittent source; previous work found that the average intermittency of O&G emissions in California was $f = 0.23$ (4). Therefore, to have a greater than 50% probability of detecting emissions at that characteristic source, at least three overpasses are needed: $p = 1 - (1 - 0.23)^3 > 0.5$. When aggregating emissions for a survey, we sum persistence-weighted source emissions. If there exist sources with less than three overflights in a survey, we sample the distribution of f values for that sector for that survey and assign it to that under-flown source before aggregating. To account for variability in sampling on aggregate emissions, we generate 1,000 Monte Carlo samples for each under-flown source for each survey.

Data, Materials, and Software Availability. Emissions data have been deposited in Zenodo (<https://doi.org/10.5281/zenodo.5606120>) (30, 31). Emission data and plume images can also be visualized and downloaded via the Carbon Mapper open data portal at <https://data.carbonmapper.org>.

- I. B. Ocko *et al.*, Acting rapidly to deploy readily available methane mitigation measures by sector can immediately slow global warming. *Environ. Res. Lett.* **16**, 054042 (2021).
- D. Zavala-Araiza *et al.*, Super-emitters in natural gas infrastructure are caused by abnormal process conditions. *Nat. Commun.* **8**, 14012 (2017).
- C. Frankenberg *et al.*, Airborne methane remote measurements reveal heavy-tail flux distribution in Four Corners region. *Proc. Natl. Acad. Sci. U.S.A.* **113**, 9734–9739 (2016).
- R. M. Duren *et al.*, California's methane super-emitters. *Nature* **575**, 180–184 (2019).
- D. H. Cusworth *et al.*, Intermittency of large methane emitters in the Permian Basin. *Environ. Sci. Technol. Lett.* **8**, 567–573 (2021).
- E. A. Kort *et al.*, Four corners: The largest US methane anomaly viewed from space. *Geophys. Res. Lett.* **41**, 6898–6903 (2014).
- Z. Qu *et al.*, Global distribution of methane emissions: A comparative inverse analysis of observations from the TROPOMI and GOSAT satellite instruments. *Atmos. Chem. Phys.* **21**, 14159–14175 (2021).
- T. Lauvaux *et al.*, Global assessment of oil and gas methane ultra-emitters. *Science* **375**, 557–561 (2022).
- J. P. Veeckind *et al.*, TROPOMI on the ESA Sentinel-5 Precursor: A GMES mission for global observations of the atmospheric composition for climate, air quality and ozone layer applications. *Remote Sens. Environ.* **120**, 70–83 (2012).
- Y. Zhang *et al.*, Quantifying methane emissions from the largest oil-producing basin in the United States from space. *Sci. Adv.* **6**, eaaz5120 (2020).
- O. Schneising *et al.*, Remote sensing of methane leakage from natural gas and petroleum systems revisited. *Atmos. Chem. Phys.* **20**, 9169–9182 (2020).
- L. Gunter *et al.*, Mapping methane point emissions with the PRISMA spaceborne imaging spectrometer. *Remote Sens. Environ.* **265**, 112671 (2021).
- D. Jervis *et al.*, The GHGSat-D imaging spectrometer. *Atmos. Meas. Tech.* **14**, 2127–2140 (2021).
- D. J. Varon *et al.*, High-frequency monitoring of anomalous methane point sources with multispectral Sentinel-2 satellite observations. *Atmos. Meas. Tech. Discuss* **2020**, 1–21 (2020).
- T. Ehret *et al.*, Global tracking and quantification of oil and gas methane leaks from recurrent sentinel-2 imagery. *Environ. Sci. Technol.* **56**, 10517–10529 (2022).
- A. K. Thorpe *et al.*, Mapping methane concentrations from a controlled release experiment using the next generation airborne visible/infrared imaging spectrometer (AVIRIS-NG). *Remote Sens. Environ.* **179**, 104–115 (2016).
- A. K. Thorpe *et al.*, Improved methane emission estimates using AVIRIS-NG and an Airborne Doppler Wind Lidar. *Remote Sens. Environ.* **266**, 112681 (2021).

ACKNOWLEDGMENTS. Funding for flight operations and/or data analysis referenced in this paper was supported by NASA's Carbon Monitoring System and Advanced Information System Technology programs as well as Rocky Mountain Institute, Environmental Defense Fund (EDF), California Air Resources Board (CARB), and the University of Arizona. Funding for Colorado overflights was provided by the Mark Martinez and Joey Irwin Memorial Public Projects Fund with the support of the Colorado Oil and Gas Conservation Commission and the Colorado Department of Public Health and Environment (CDPHE). The Carbon Mapper team also acknowledges the support of their sponsors including the High Tide Foundation, Bloomberg Philanthropies, Grantham Foundation, and other philanthropic donors. We thank colleagues at CARB, CDPHE, Colorado State University, University of Utah, EDF, and Pennsylvania Department of Environmental Protection for input on survey design and analysis for the California, Colorado, Utah, Permian, and Pennsylvania studies, respectively. Portions of this work were carried out at the Jet Propulsion Laboratory, California Institute of Technology, under a contract with the National Aeronautics and Space Administration (80NM0018D0004). We thank Dan Zimmerle for on-the-ground insights during the Denver-Julesburg flights. We thank Daniel Varon for conversations regarding inversion frameworks and validation. The Global Airborne Observatory (GAO) is managed by the Center for Global Discovery and Conservation Science at Arizona State University. The GAO is made possible by support from private foundations, visionary individuals, and Arizona State University.

Author affiliations: ^aArizona Institutes for Resilience, University of Arizona, Tucson, AZ 85721; ^bCarbon Mapper, Pasadena, CA 91105; ^cJet Propulsion Laboratory, California Institute of Technology, Pasadena, CA 91109; ^dCenter for Global Discovery and Conservation Science, Arizona State University, Tempe, AZ 85281; and ^eEnvironmental Defense Fund, Austin, TX 78701

- B. Fasoli, J. C. Lin, D. R. Bowling, L. Mitchell, D. Mendoza, Simulating atmospheric tracer concentrations for spatially distributed receptors: Updates to the Stochastic Time-Inverted Lagrangian Transport model's R interface (STILT-R version 2). *Geosci. Model Dev.* **11**, 2813–2824 (2018).
- M. Maasackers *et al.*, Gridded national inventory of US methane emissions. *Environ. Sci. Technol.* **50**, 13123–13133 (2016).
- T. R. Scarpelli *et al.*, A global gridded (0.1° × 0.1°) inventory of methane emissions from oil, gas, and coal exploitation based on national reports to the United Nations Framework Convention on Climate Change. *Earth Syst. Sci. Data* **12**, 563–575 (2020).
- S. Ma *et al.*, Satellite constraints on the latitudinal distribution and temperature sensitivity of wetland methane emissions. *AGU Adv.* **2**, e2021AV000408 (2021).
- US Environmental Protection Agency, Greenhouse Gas Inventory Data Explorer. <https://cfpub.epa.gov/ghgdata/inventoryexplorer/#allsectors/allsectors/methane/inventsect/current>. Accessed 15 December 2021.
- R. A. Alvarez *et al.*, Assessment of methane emissions from the U.S. oil and gas supply chain. *Science* **361**, 186–188 (2018).
- MesoWest, KGXY station weather data. https://mesowest.utah.edu/cgi-bin/droman/download_api2.cgi?stn=KGXY&year1=2022&day1=31&month1=1&hour1=14&timetype=LOCAL&unit=0. Accessed 31 January 2022.
- D. R. Lyon *et al.*, Concurrent variation in oil and gas methane emissions and oil price during the COVID-19 pandemic. *Atmos. Chem. Phys.* **21**, 6605–6626 (2021).
- ExxonMobil, ExxonMobil field testing new comprehensive methane monitoring technologies (April 9, 2020). https://corporate.exxonmobil.com/News/Newsroom/News-releases/2020/0409_ExxonMobil-field-testing-new-comprehensive-methane-monitoring-technologies. Accessed 1 February 2022.
- California Department of Food and Agriculture, Report of funded projects (2015 – 2020). https://www.cdffa.ca.gov/oeif/dddrrp/docs/DDRDP_Report_March2021.pdf. Accessed 28 January 2021.
- D. J. Jacob *et al.*, Quantifying methane emissions from the global scale down to point sources using satellite observations of atmospheric methane. *Atmos. Chem. Phys.* **22**, 9617–9646 (2022).
- V. Yadav *et al.*, Spatio-temporally resolved methane fluxes from the Los Angeles Megacity. *J. Geophys. Res. D Atmospheres* **124**, 5131–5148 (2019).
- D. H. Cusworth *et al.*, Methane plumes from airborne surveys 2020-2021 (1.0) [Data set]. Zenodo. <https://doi.org/10.5281/zenodo.5606120>. Deposited 27 October 2021.
- D. H. Cusworth *et al.*, Methane plumes for NASA/JPLU/Arizona/ASU Sep-Nov 2019 Permian campaign [Data set]. Zenodo. <https://doi.org/10.5281/zenodo.5610307>. Deposited 28 October 2021.